Final Technical Report- 11/30/07

Influence of Surface Roughness on Polymer Drag Reduction
HR0011-06-1-0057

Prof. Steven L. Ceccio (Principal Investigator)
Mechanical Engineering, University of Michigan, Ann Arbor

Prof. David R. Dowling (Co-Principal Investigator)
Mechanical Engineering, University of Michigan, Ann Arbor

Prof. Marc Perlin (Co-Principal Investigator)
Naval Architecture and Marine Engineering, University of Michigan, Ann Arbor

Prof. Michael Solomon (Co-Principal Investigator)
Chemical Engineering, University of Michigan

Background: This effort accompanied the DARPA Friction Drag Reduction Program (ATO/TTO) effort at the University of Michigan funded under contract HR-0011-04-1-001 "High Reynolds Number Micro-bubble and Polymer Drag Reduction Experiments" for flows over smooth surfaces. The details of that effort can be found in the final technical report for that project. The purpose of the additional investigation was to examine the physics and engineering of friction drag reduction methods for turbulent boundary layers (TBL) found in hydrodynamic flows over *rough surfaces*. Two methods of friction drag reduction (FDR) were examined:

- *Polymer Drag Reduction*- solutions containing extensible, long-chain molecules are injected into a TBL. The polymer molecules interact with the underlying turbulent flow and lead to a reduction of the correlated velocity fluctuations and, hence, a reduction of the turbulent transport of momentum across the TBL. This leads to local drag reduction of up to ~70% for TBL flows over smooth surfaces compared to a flow without polymer injection.

- *Air Layer Drag Reduction*- air is injected into the TBL with the aim of creating a stable gas layer of very high void fraction (> 80% void fraction), separating the liquid flow from the solid surface. This results in friction drag reductions of over 80% compared to the friction drag without air layers.

Reduction of drag on marine transportation systems can reduce fuel cost and increase ship performance, including maximum speed, range between refueling, and increased payload. Currently, reduction in fuel cost is the primary driving force behind drag-reduction research efforts because the world's non-military fleet consumed nearly 280 million tons of fuel as of 2006 and, as of 2005, the U.S. military was the world's largest consumer of diesel fuel.

1

20080131286

There are three primary sources of drag that a ship encounters (form, wave, and viscous/skin-friction drag) and figure 1 shows a typical plot of the drag component ratio versus the Froude number with C_D and Fr defined below.

$$C_D = \frac{D}{\frac{1}{2}\rho U^2}$$

$$Fr = \frac{U}{\sqrt{gL}}$$

Here ρ is the fluid mass density, g is the acceleration of gravity, L is the length of the ship, U is the forward speed of the vessel, and D is the drag force. Modifications to the hull shape is the most common approach for reduction in form or wave drag, however other approaches are necessary for reduction of viscous drag.
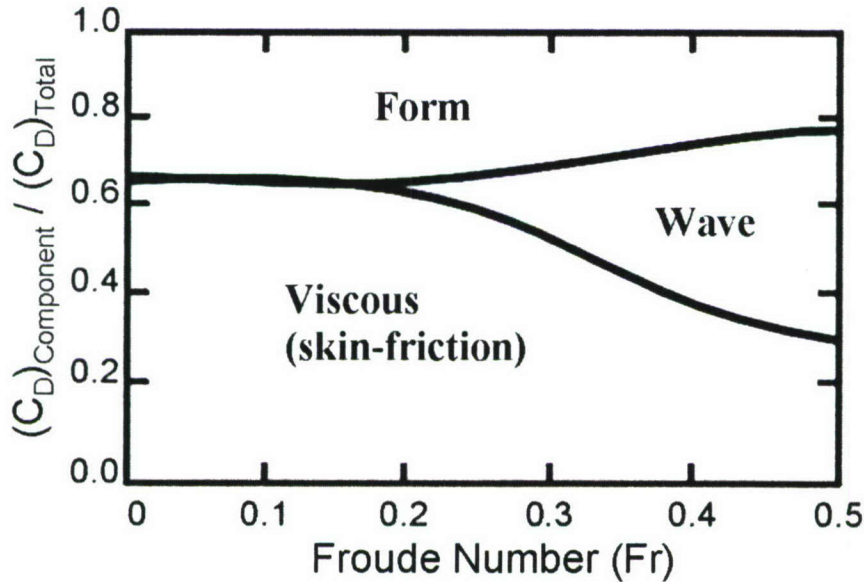

Figure 1: Drag component ratio as a function of Froude number for a typical ship.

Reduction of the viscous or skin-friction drag can be accomplished by either active or passive techniques. Passive methods, including hydrophobic surfaces and riblets, involve modifying the ship surface to reduce velocity gradients there. These methods are limited often by a combination of a lack of success in real seas, and the required continual cleaning or maintenance of the ship surface. Active methods involve injection of a substance from the ship surface that modifies the flow conditions in the near-wall region of the boundary layer resulting in a reduction in skin-friction drag. Substances used for active reduction in skin-friction drag include air, surfactants, and polymer solutions. While active methods avoid the disadvantages associated with passive methods, they are limited by power requirements to deliver the drag reducing agent to the flow and space requirements on the ship. Although a number of passive and active methods have been

investigated by our research group, the current work focuses only on active drag reduction with polymer solution injection.

Previous Work on Polymer Drag Reduction: Polymer drag reduction (PDR) methods have been shown to reduce skin-friction drag by up to 75% in lab scale experiments. Knowledge that dilute polymer solutions added to Newtonian flows can reduce skin-friction drag has been known for nearly sixty years since Toms (1949) first discovered it. In spite of decades of study, the underlying mechanism that produces the reduction in drag remains uncertain. However, recent work by Dubief *et al.* (2004) has produced a detailed description of a possible mechanism for reducing drag that is consistent with observations from recent work (Warholic *et al.*, 1999, Ptasinski *et al.*, 2003, and White *et al.*, 2004). The mechanism involves the storage of energy by the polymer around near-wall vortices (stretching) and the release of energy in an organized fashion to near-wall streaks (recoiling). Dubief *et al.* modified the near-wall turbulent regeneration cycle proposed by Jiménez and Pinelli (1999) for Newtonian flow to include the effects of the polymer solutions. This ultimately creates a balance between viscous, Reynolds, and polymer stresses in the near-wall region. The modified turbulence regeneration cycle leads to enhanced stream-wise velocity fluctuations, decreased wall-normal velocity fluctuations, and increased spacing between stream-wise vortices.

The vast majority of research studies for PDR have focused on internal flows, which has produced a good understanding of many of the primary parameters influencing PDR. Virk (1975) gives a comprehensive overview of these key parameters, including pipe diameter, polymer concentration, polymer molecular weight, and random coil size. This knowledge base has created numerous pipe flow applications for PDR, many of which are discussed in Sellin *et al.* (1982a,b), but has failed to produce an economical solution for large scale exterior flows such as the flow over a large ship. The primary problem with external flows is mixing always takes place, even at maximum drag reduction (MDR).

More recently studies have focused on turbulent boundary layers (TBL) in an attempt to determine if there exists a potential injection scheme that would make PDR economical for large scale ships. Studies have investigated PDR on TBL flows at downstream-distance based Reynolds numbers up to 45 million (Vdovin and Smol'yakov, 1981) and speeds up to 16.8 m/s (Petrie *et al.*, 1996). However nearly all previous studies on PDR in a TBL have been with hydro-dynamically smooth surfaces, and the presence of roughness will only increase the mixing rate. One exception is Petrie *et al.* (2003) that investigates several surface roughnesses by applying different grit sandpaper to their model. They report some instances where the roughness hindered polymer performance as well as some cases where it improved the performance. This inspired the current investigation to determine under what conditions, if any, does surface roughness decrease polymer degradation.

PDR over Rough Surfaces: Results from data sets that have been processed thus far are shown and briefly discussed, and at the end of this section a list of data sets currently being processed is given.

Test Facility- Testing was performed at the U.S. Navy's William B. Morgan Large Cavitation Channel (LCC) in Memphis, TN. The LCC is the world's largest low-turbulence (free-stream turbulence < 0.5%), recirculating water tunnel. The test section dimensions are 16 m (length) and 3.05 m by 3.05 m (height and width) cross section. The free-stream tunnel speeds tested ranged from 6.7 to 20 m/s. Additional LCC facility details can be found in Etter *et al*. (2005).

HIPLATE Model- The test model, termed HIPLATE (HIgh Reynolds number, flat PLATE), is 12.9 m long, 3.05 m wide, and 18 cm thick, has a 4:1 ellipse at the leading edge, and 15° full angle truncated wedge at the trailing edge. Figure 2 shows a schematic of the model with details of the instrumental suite employed. The model was mounted slightly below the centerline of the LCC test section, spanned the entire width of the LCC test section, and had the working surface faced downward, schematically shown in Figure 3. Initially the surface was polished 304 stainless steel yielding a RMS roughness, k < 0.4 µm, which was sufficient for the model to be considered hydro-dynamically smooth at all test speeds. Then the entire test model surface was roughened using epoxy paint (High Build Semi-Gloss 97-130, Aquapon) with glass bead grit. The particles were tightly packed producing a sand grain type roughness. Based on the skin-friction measurements and assuming a fully roughened surface, the first 75% of the model was very uniform yielding an average roughness height, k, between 400 and 600 μm. The remaining 25% of the model was rougher with k ranging from 800 to 1100 μm.
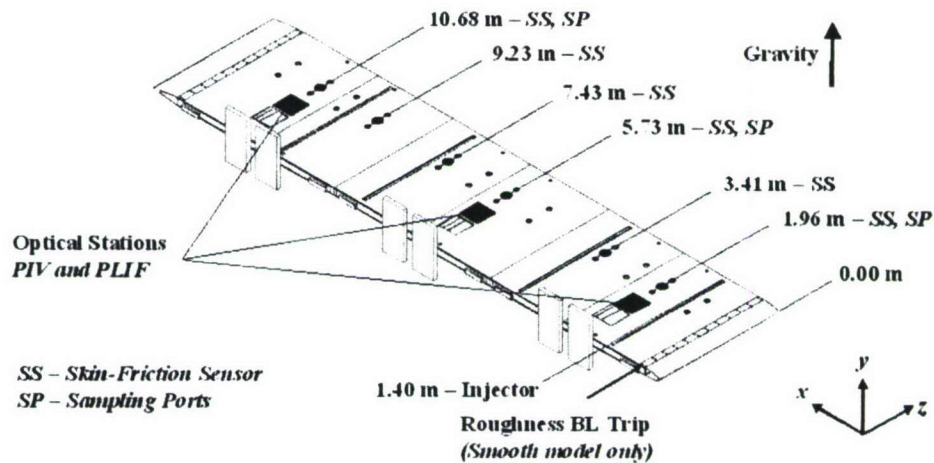

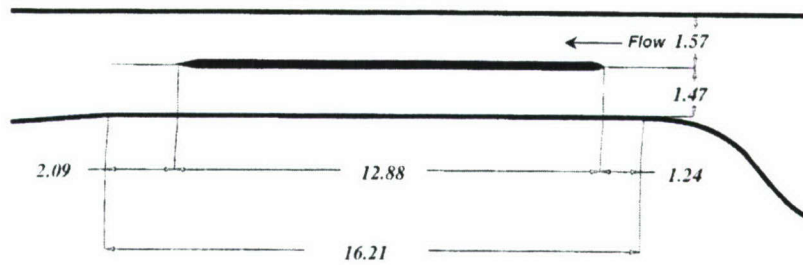**Figure 2: HIPLATE test model schematic with the injection and measurement locations**

Figure 3: Schematic of the HIPLATE mounted in the LCC test section

Polymer Injector- The test model was fitted with a single injector located 1.40 m downstream of the leading edge. This was a slot injector inclined at a shallow 5.7° from the model surface and contracting at a full angle of 6.1°. The downstream edge was broken to give a convex downstream surface that produced a 1.5 cm opening in the stream-wise direction on the test model surface. Polymer was delivered to a manifold thru 40 evenly spaced ports along the injector span. Within the manifold, three layers of baffles and porous brass screens generated a pressure drop to ensure even span-wise distribution of polymer into the slot. However, due to the viscoelastic nature of the polymer and the injector geometry, polymer was not injected into the flow uniformly. To remedy this a 6.4 cm wide strip of porous material was added 1.9 cm upstream of the knife edge in the injector throat to produce a pressure drop near the flow entrance. This corrected the problem and based on dye injection experiments produced span-wise uniform distribution of polymer into the flow. Figure 4 shows a cross-sectional schematic of the injector.
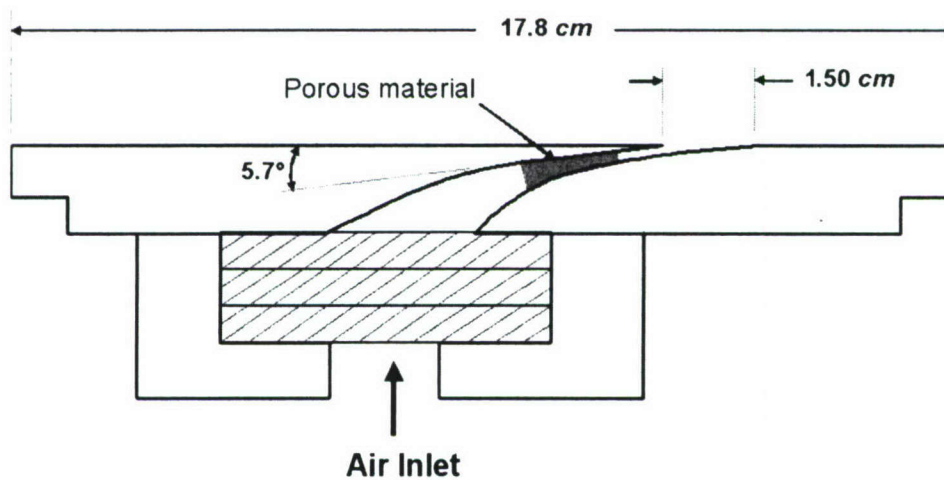

Figure 4: Schematic view of the slot injector.

Skin-Friction Data- Integrated skin-friction measurements were made with "floating plate" type drag balances. Six sensors were stream-wise located along the test model. The balances were originally designed by researchers at Pennsylvania State University – Applied Research Laboratory and then modified by UM. The floating plate is 15.2 cm in diameter, 0.79 cm thick, and made of 17-4PH stainless steel. The floating plate was

rigidly fixed to a beryllium copper flexure that was instrumented with a full wheat-stone bridge of semiconductor strain gages. The floating plate and the housing were flush mounted using an eight point leveling system. There was a 60 ± 20 μm gap between the floating plate and the housing. A skin-friction sensor is schematically shown in Figure 5.
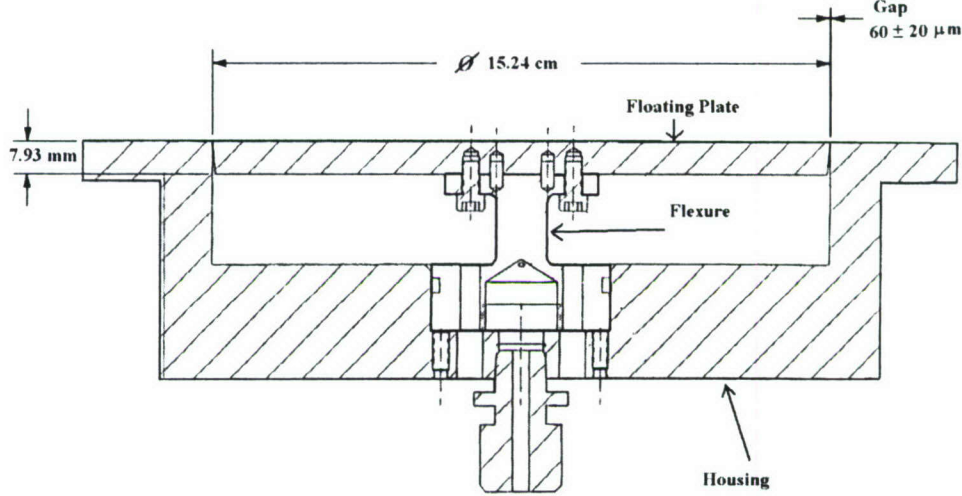

Figure 5: Cross sectional schematic view of the skin-friction sensor including the floating plate, flexure, and housing.

The strain gages were excited using a Vishay signal-conditioning amplifier (Model 2310, Vishay Measurement Group). The sensor outputs were low-pass filtered at 10 Hz and amplified with the same Vishay unit, then sampled at 50 Hz with a National Instruments NI-DAQ data acquisition board and LabView virtual instrument.

The sensors were calibrated between zero and two pounds for testing on the smooth test model and between zero and three pounds for the rough model. All calibrations were performed *in situ*. The floating plate was fixed to a second load cell (Model LCEB-5, Omega Engineering) positioned downstream on a linear traverse by a cable and suction cup applied to the floating plate. The second load cell was calibrated by hanging weights from it prior to skin-friction sensor calibrating. The linear traverse would move the precision load cell, and thus change the tension on the cable. Between three and five different loads would be applied to each sensor for the calibration. Multiple calibrations were performed on the skin-friction sensors to confirm the sensor stability and repeatability of the calibration method.

Figure 6 shows the baseline (non-injection) skin-friction coefficients, C_{fo} obtained from the current smooth model experiment (HIPLATE V) and a prior experiment on the same smooth model (HIPLATE IV), where $C_{fo} = \tau_{wo} / \frac{1}{2}\rho U_\infty^2$. Also plotted with the current baseline results are the best-fit curve for HIPLATE IV and V data sets and the Schultz-Grunow (1941) curve:

$$C_{fo} = 0.370\log^{-2.584}\left(\mathrm{Re}_X\right) \tag{1}$$

6

where $Re_x = U_\infty X/v$, X is the downstream distance from the model leading edge and v is the kinematic viscosity. Both data sets obtained from the HIPLATE model are in good agreement with the Schultz-Grunow (1941) friction line.
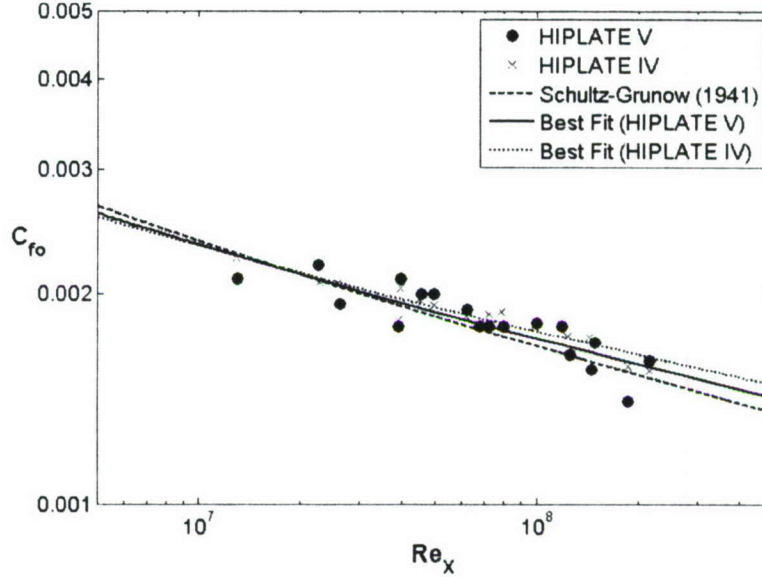
Figure 6: Baseline skin-friction curves for the smooth HIPLATE model. Included in the plot are the Schultz-Grunow (1941) friction curve and the best-fit curves for data collected during HIPLATE IV and V.

Figure 7 shows the baseline (non-injection) results obtained from the rough model. The particles embedded in the epoxy coating were tightly packed giving an average roughness height, $k \sim 460 \pm 120\ \mu m$. This k value was uniform across the first nine meters of the plate, however along the last four meters, the coating was not applied as uniformly resulting in approximately double the k value. These skin-friction coefficient curves were also used to estimate the average roughness height by assuming the surface was fully rough, which is supported by the Reynolds number independence of the skin friction coefficient at a given downstream location. The surface roughness was inferred from the measured drag after examining White's and Schlichting's friction curves for fully rough flow over a flat plate (White, 1991).

$$C_{fo} \approx \left[1.4 + 3.7 \log_{10}\left(\frac{X}{k} \right) \right]^{-2} \qquad \text{White} \qquad (2)$$

$$C_{fo} \approx \left[2.87 + 1.58 \log_{10}\left(\frac{X}{k} \right) \right]^{-2.5} \qquad \text{Schlichting} \qquad (3)$$

This method yielded average roughness heights of 400, 550, 580, 1100, and 830 μm at X = 1.96, 5.94, 7.43, 9.23, and 10.7 m, respectively. These results are consistent with a visual examination of the surface.
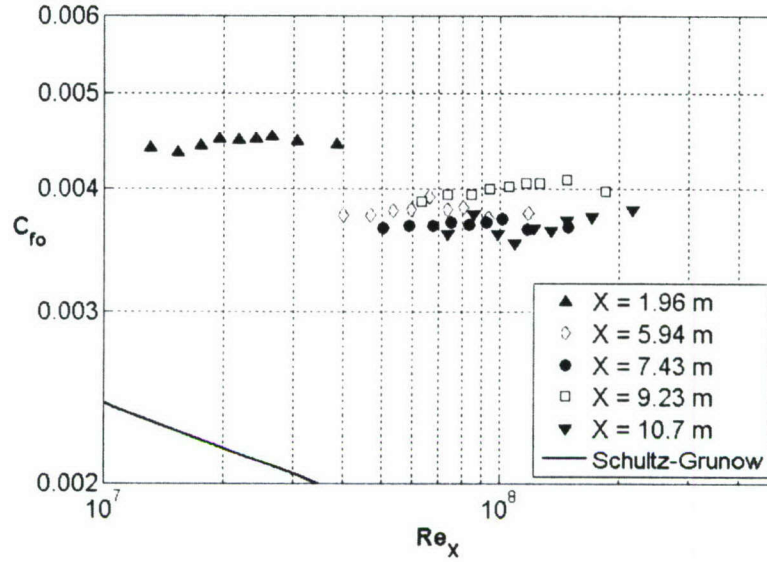
7

Figure 7: Baseline skin-friction curves for the HIPLATE model with the roughened surface.

Skin-Friction Drag Reduction- Reduction in the skin-friction drag is presented as a percentage drag-reduction, %DR, defined by (4), where τ_{wo} is the shear stress without gas injection and τ_w is the skin friction with polymer injection.

$$\%DR = \left(1 - \frac{\tau_w}{\tau_{wo}}\right) 100\% \qquad (4)$$

All results shown were obtained with a single, commonly used polymer, poly-ethylene oxide (PEO) water-soluble resin (WSR) with a nominal mean molecular weight of 4 million, herein referred to as WSR-301 (Dow Chemical Company). While a number of injection conditions were investigated for both the smooth and rough models, a single injection condition was used as the primary test condition and will be discussed almost exclusively in the results. The injected polymer concentration was 4000 wppm and injected at 10 Q_i / Q_s, where Q_i is the volumetric flux of polymer per unit span and Q_s is an estimate of the liquid flow in the near-wall region of the boundary layer. Wu and Tulin (1972) established this value as 67.3ν by assuming a linear velocity profile and integrating the stream-wise velocity over the range of $0 < y^+ < 11.6$, y^+ is the wall normal distance normalized with the viscous wall unit $l_v = v\sqrt{\rho/\tau_{wo}}$, where ϱ is the fluid density.

Figure 8 shows the %DR versus the downstream distance from the injector for the primary injection condition for both the smooth and rough model at the three primary test speeds, 6.8, 13.5, and 20.0 m/s. The first observation is that the rough surface significantly decreases the downstream persistence of PDR at all test speeds. The single improved data point with roughness occurred at the lowest test speed, 6.8 m/s, and the

8

closest measurement to the injector. This supports the findings of Petrie *et al.* (2003) that observed some improvement with surface roughness with measurements near the injection location. However it appears that this phenomenon is confined to the near injector region. Even more alarming is the complete absence of drag reduction at the top speed, 20 m/s, within the first meter of injection. It should be noted that while the presence of polymer can increase the drag due to the higher viscosity, the negative values shown in Figure 8 are within the uncertainty of the measurement.
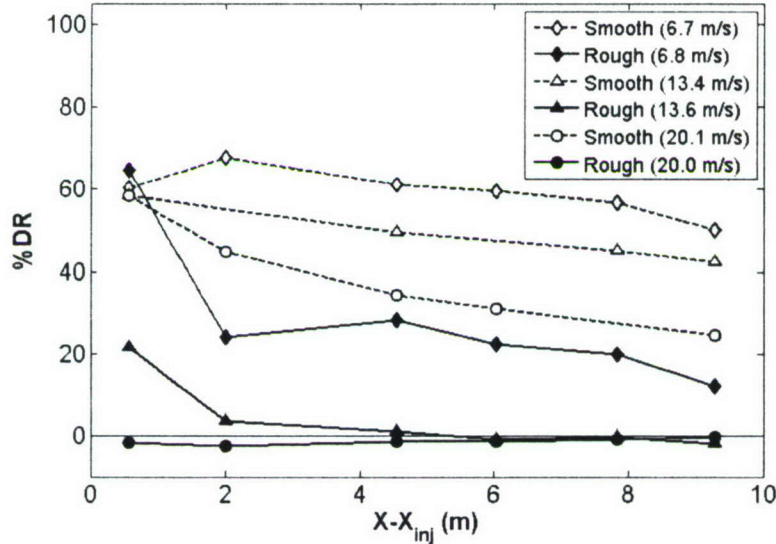

Figure 8: Comparison of the drag reduction results for the smooth and rough models. Shown are the three primary test speeds with a single injection condition (4000 wppm and 10 Q$_i$/Q$_s$).

In an attempt to present more a complete picture of the data acquired during this experiment the use of the K-factor introduced by Vdovin and Smol'yakov (1981) will be employed. The K-factor, given in (5), is a simple scaling relationship based on the flux of polymer into the boundary layer, downstream distance, and flow-speed.

$$K = \frac{Q_i C_i}{\rho U_\infty \left(X - X_{inj}\right)} \quad (5)$$

Here C_i is the injected polymer concentration in units of density, ρ is the fluid density, and U_∞ is the free-stream speed. While the use of the K-factor has not been an ideal scaling variable, it has been a useful tool for organizing/comparing large amounts of data from a wide variety of injection conditions for a single polymer type.

Figure 9 shows %DR versus K for all test conditions on both the smooth and rough models. There is significant scatter in the data, but it is apparent from the plot that for a given K value, the rough model consistently performed worse than the smooth model. The only exceptions are a few data points that appear to overlap the rough model data set, but all these data points correspond to conditions closest to the injector and are influenced by an incubation region (see Figure 8 smooth model data for 6.7 m/s and note the rise in %DR going downstream).
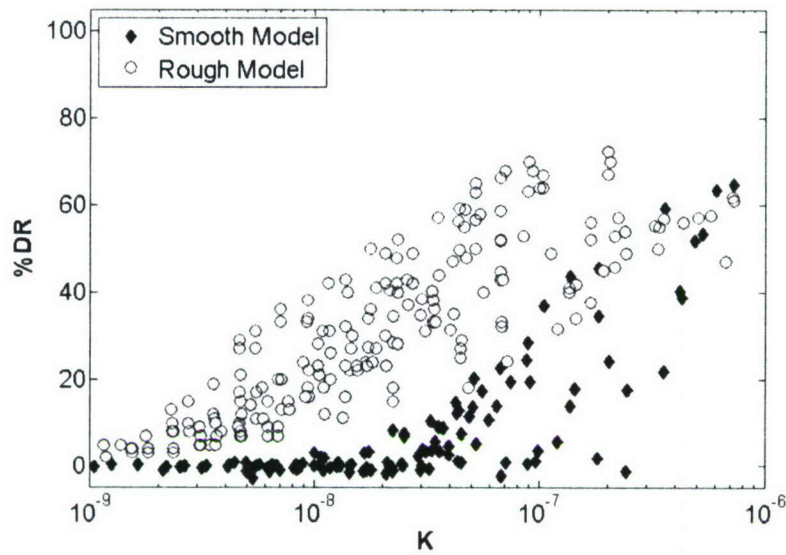
Figure 9: Comparison of all data collected on the smooth and rough HIPLATE model.

While Petrie *et al.* (2003) observed improvements to drag reduction with the roughened surfaces, their results are still in agreement with our current findings. Taking their largest roughness data set (60-grit sand paper) and making a K-plot with similar velocity ranges, and both data sets appear to fall to zero %DR at nearly the same K value. It should be noted that Petrie *et al.* K values will be shifted slightly to the left compared with ours due to their use of the downstream distance defined to the downstream edge of their sensing element, which spanned their entire working surface.
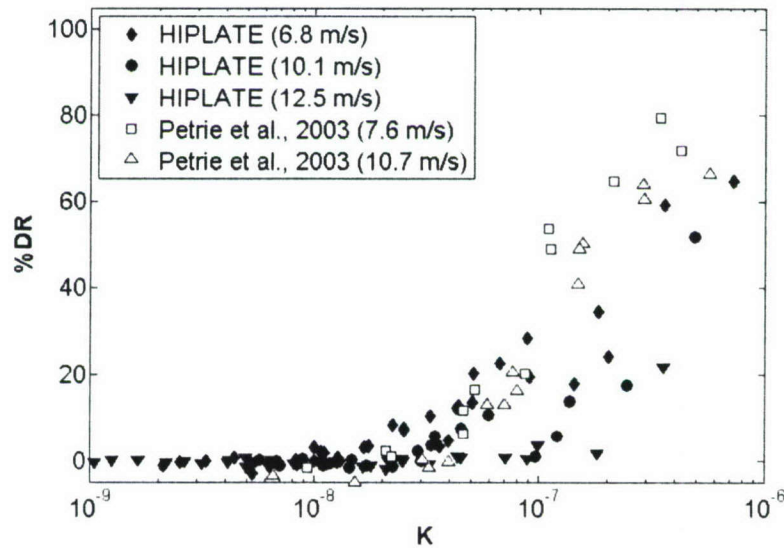

Figure 10: K-plot comparing results obtained from the rough HIPLATE with data obtained from Petrie *et al.* (2003) with a 60-grit rough surface.

Polymer Sampling- The data collected for the sampling experiments were only obtained for the primary injection condition, 4000 wppm WSR-301 at 10 Q_i / Q_s. Analysis of the drawn samples was performed using either a pressure drop tube or a cone and plate rheometer (AR1000, TA Instruments), depending on the sample concentration. Presented in this section are the processed results from the individual apparatuses, but further analysis is required to appropriately compare results made with different apparatuses.

The test model was fitted with six sampling ports for collection of flow samples from the near-wall region of the boundary layer (two at each downstream location shown in Figure 2). The collected samples were used to determine if polymer degradation was caused by the turbulent flow. This was accomplished by injecting dyed polymer (Rhodamine 6G dye, Sigma-Aldrich) and drawing samples through the sampling ports. A spectrophotometer was used to determine the dye concentration of the test sample. Then a control sample was prepared by diluting to the measured concentration using the same stock solution used for the injection and tunnel water. Lastly, depending on the concentration of the test sample either a cone and plate rheometer or a pipe setup similar to the setup used in Virk (1975) was used.

The six sampling ports were positioned at three stream-wise locations (X = 1.96, 5.94, 10.68 m). At each stream-wise location two ports were plumbed together within the test model and a single 2.54 cm inner diameter hose exited the model for sample collection. The sampling port was made from an 11.4 cm diameter PVC disk and flush mounted on the test model surface. A rectangular opening 5.6 cm (cross-stream) x 0.64 cm (stream-wise) was positioned at the center of the PVC disk for collection of flow samples. Each opening filled a 63.4 cm^3 cylindrical interior cavity that fed the 2.54 cm inner diameter hose. At each stream-wise position the two ports were connected with a wye pipe fitting that had the single exit line for collection.

Table 1 gives a summary of the test conditions performed on the smooth model with the free-stream velocity, downstream distance from the injector, sample mass flow rate, sample polymer concentration, and apparatus used to analyze the drawn sample. Prior to the experiment it was confirmed that the sampling method did not cause degradation when sampling below 0.65 kg/s. In addition the sample drawn at 6.7 m/s from $X-X_{inj}$ = 0.56 (Figure 11 – top) experienced no degradation indicating that the polymer delivery and injection setup was not responsible for polymer degradation.

Table 1: Summary of sampling conditions tested on the smooth HIPLATE.

U_∞ (m/s)	$X-X_{inj}$ (m)	Q_s (kg/s)	C_s (wppm)	Apparatus
6.7	0.56	0.57	350	Rheometer
6.7	4.54	0.19	15	½" Pressure Drop Tube
6.7	9.28	0.34	5.6	¼" Pressure Drop Tube
13.4	0.56	0.65	280	Rheometer
13.4	4.54	0.24	5.9	½" Pressure Drop Tube
13.4	9.28	0.34	2.1	¼" Pressure Drop Tube
20.1	0.56	0.20	38	Rheometer

Figure 11 shows the results obtained for the 6.7 m/s conditions at the three sampling locations. While no significant degradation was observed for the sample drawn at $X-X_{inj} = 0.56$, both further downstream locations exhibited polymer degradation. Direct comparison between stations is not possible due to each sample being tested in separate apparatuses.
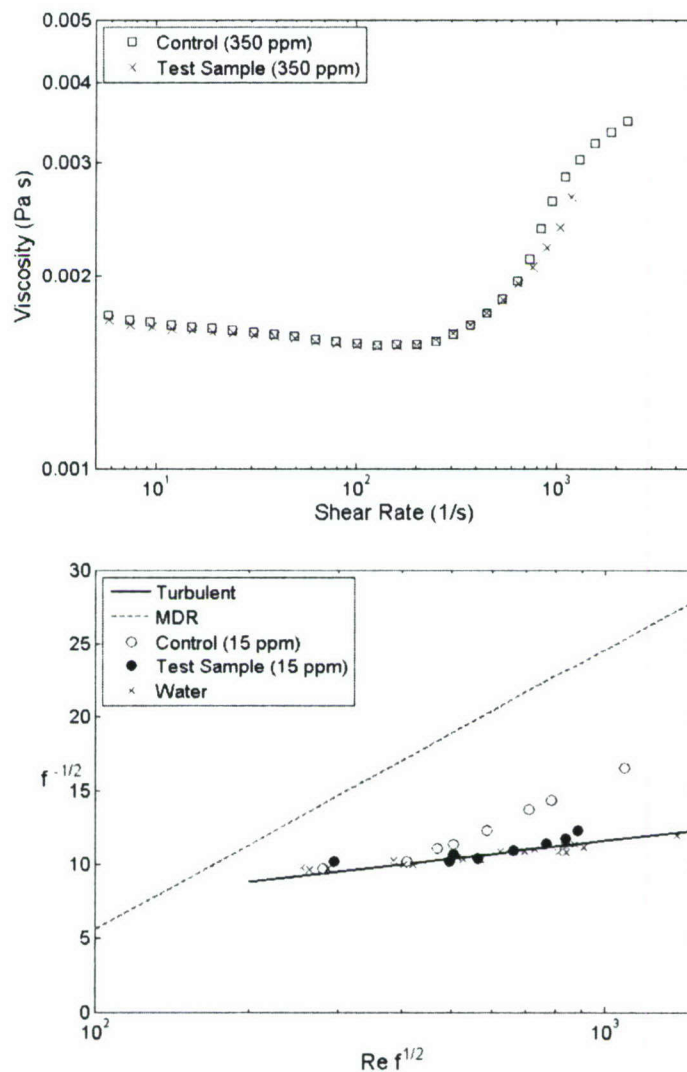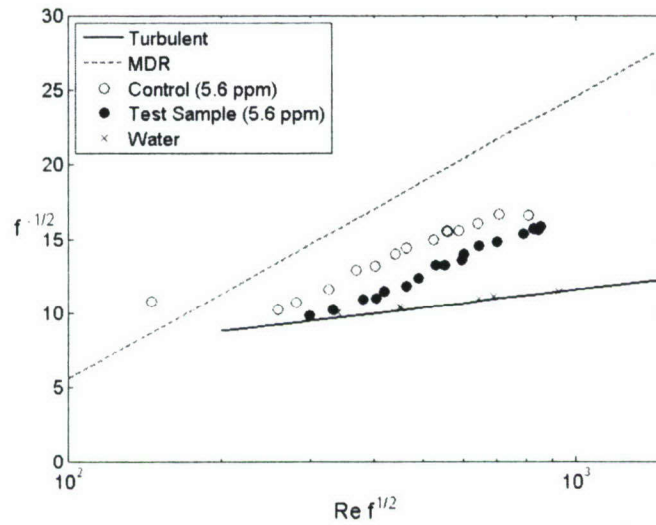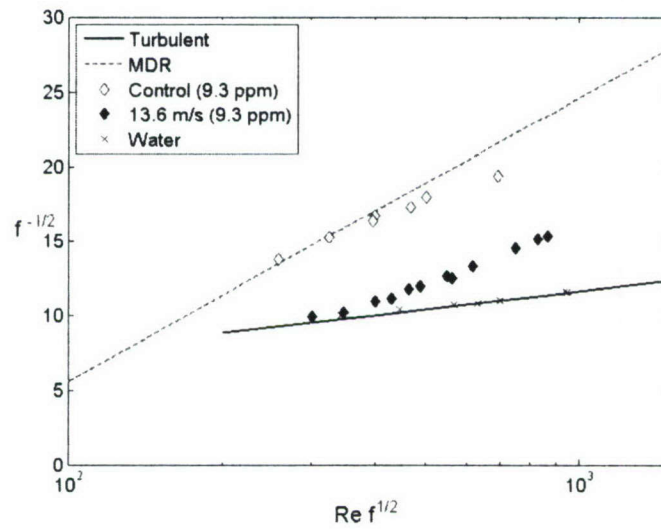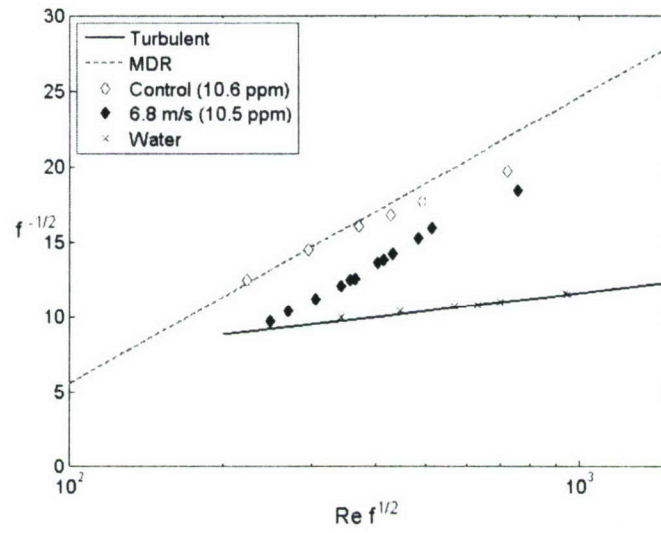
Figure 11: Sampling results from the smooth model taken at 6.8 m/s from X-X_{inj} = 0.56 (top), X-X_{inj} = 4.54 (middle), and X-X_{inj} = 9.28 (bottom). All sampling runs had the same injection condition (4000 wppm and 10 Q_i/Q_s).

Sampling on the rough model was less thorough than with the smooth model due to time limitations at the test facility. Thus one location, X-X_{inj} = 0.56, was selected along with three test speeds. In addition the rheometer was unavailable and the pressure drop tube had to be re-assembled. Thus all three samples were tested in the same apparatus by diluting the drawn samples to approximately 10 wppm (the concentration required to reach the maximum drag reduction asymptote, MDR, in the ¼" tube). Table 2 summarizes the conditions tested on the rough model.

Table 2: Summary of sampling conditions tested on the rough HIPLATE model.

U_∞ (m/s)	X-X_{inj} (m)	Q_s (kg/s)	C_s (wppm)	C_{test} (wppm)	Apparatus
6.8	0.56	0.24	260	10.5	¼" Pressure Drop Tube
13.6	0.56	0.30	46	9.3	¼" Pressure Drop Tube
20.0	0.56	0.20	8.8	8.8	¼" Pressure Drop Tube

Figure 12 shows the results obtained from the pressure drop tube analysis, which can be compared directly due to the same tube and nearly the same test concentrations. By focusing on the onset of drag reduction (point where the curves leave the turbulence line) and the slope increment (slope of the curve after the onset of drag reduction) one can determine the relative effectiveness of the polymer solution. The 6.8 m/s case has significant degradation from the control, but still lies in the polymeric region of the plot; at 13.6 m/s more degradation has occurred, but the sample curve still lies above that of pure water; and finally at 20.0 m/s the test sample appears to be nearly identical to that of pure water. This indicates that polymer degradation is the primary mechanism causing the reduction in downstream persistence of PDR.
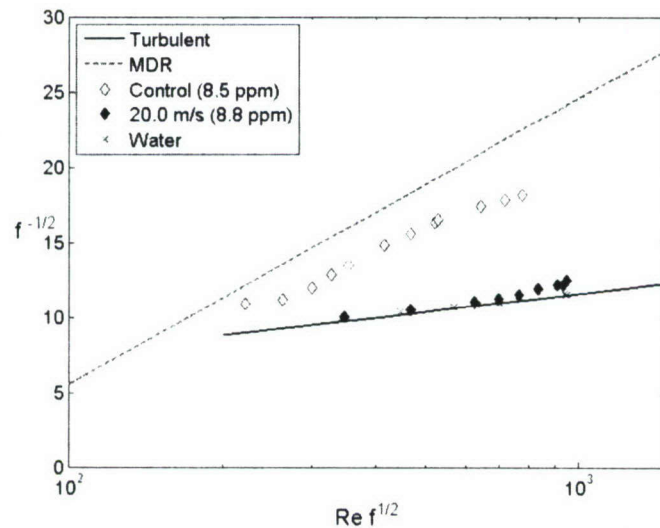
Figure 12: Sampling results from the rough model drawn from X-X$_{inj}$ = 0.56 at 6.8 m/s (top), 13.6 m/s (middle), and 20.0 m/s (bottom). All sampling tests had the same injection condition (4000 wppm and 10 Q$_i$/Q$_s$).

Conclusions for PDR Over Rough Surfaces: The presence of roughness results in increased mixing of the polymer solutions and increased polymer degradation. The increased mixing can lead to a short region of increased FDR compared to the smooth conditions very near the injector. However, the increased mixing rate ultimately leads to the rapid decay of the near-wall polymer concentration and, hence, the friction drag reduction. The presence of the roughness also led to an increased level of polymer degradation. Both of these effects will result in a significantly increased level of polymer expenditure needed to achieve the equivalent levels of friction drag reduction over a long smooth surface.

Air Layer Drag Reduction over Rough Surfaces: If enough air is injected into the TBL, the gas can coalesce into a layer under the influence of buoyancy. This was observed in the first round of MBDR testing at lower speeds, where the friction drag was reduced by over 80% over the full stream-wise extent of the test model. In the follow-on experiments, we observed this Air Layer Drag Reduction (ALDR) at higher speeds, with increased gas flux. The critical gas flux and dynamics of the air layers were examined for flow over the smooth and roughed HIPLATE. This work has been submitted for publication in the *Journal of Fluid Mechanics*:

- Belbing, B. R., Winkel, E. S., Lay, K. A., Ceccio, S. L., Dowling, D. R., and Perlin, M., "Bubble-Induced Skin-friction Drag Reduction and the Abrupt Transition to Air-layer Drag Reduction," *Journal of Fluid Mechanics*, (**submitted**) (2008)

Two independent experiments were conducted at the LCC, the world's largest low-turbulence (free-stream turbulence < 0.5%), recirculating water tunnel. The test section dimensions are 16 m (length) and 3.05 m square cross section. The free-stream tunnel speeds tested ranged from 6.5 to 20 m/s. Additional LCC facility details can be found in Etter *et al.* (2005). These experiments were conducted as part of DARPA's Friction Drag Reduction (FDR) program. Details of the first two phases of experiments can be found in Sanders *et al.* (2006). The experiments presented here are products of Phases IV and V of the testing. Phase V testing was divided into two sections: Phase Va had a smooth model surface, and Phase Vb had a roughened model surface.

Phase IV was designed to investigate the BDR phenomenon by varying injector design, injection location, and bubble size. In addition compound injection was tested for synergetic effects on downstream persistence. The model was fitted with two injection locations, X_{inj} = 1.38 and 3.73 m measured from the leading edge. Two different types of injectors (porous-plate or slot injector) were tested and both spanned the center 2.65 m of the model (~90% of the model span). The porous-plate injector consisted of a slot inclined at a mean angle of 20° from the test surface and contracting at a full angle of 10°. The slot was then fitted with a 2.0 mm thick piece of porous (40μm mean pore diameter) sintered stainless steel (Mott Corporation). The porous material was flush with the test surface extending 2.5 cm in the stream-wise direction and was epoxied to the injector to ensure that all injected air passed through it. This was the same design employed in the experiments of Sanders *et al.* (2006). The slot injector was inclined at 12° from the working surface and had a constant throat gap of 5.8 mm. This produced a stream-wise opening of 2.8 cm on the test surface.

Phase V was an ALDR experiment that used a single injector located 1.40 m downstream of the leading edge. This was a slot injector inclined at a shallow 5.7° from the model surface and contracting at a full angle of 6.1°. The downstream edge was broken so that it had a convex Coanda surface and produced a 1.5 cm opening on the test model surface. Since the objective of ALDR would be to reduce the skin friction drag on a naval ship that was not hydro-dynamically smooth, Phase V investigated the effects of roughness on ALDR. In Phase Va the model was hydro-dynamically smooth to check any effects on ALDR from the change in slot injector geometry. Phase Vb had the entire model test surface roughened using epoxy paint (Aquapon High Build Semi-Gloss Epoxy 97-130) with glass bead grit blown into the epoxy. The particles were tightly packed giving an average roughness height, Ra ~ 460 ± 120 μm. This Ra value was uniform across the first 9 m of the plate, but the last 4 meters was not applied as uniformly resulting in approximately double the Ra value.

The mass flow rate of air being injected was monitored with thermal mass flow meters (Series 640S Steel-Mass, Sierra Instruments). They were insertion type meters consisting of two probes, one for measuring velocity and one for measuring temperature. The meter was mounted at the center of a 6.3 cm inner diameter, straight steel pipe. To ensure fully developed flow at the flow meters they were mounted 30 inner diameters (1.90 m) downstream and 10 inner diameters (0.63 m) upstream of any line junctions. The meters were factory calibrated from 0-820 SCFM in an operating range of 0-50 psig and 50-130

°F. Each flow meter had an analog voltage output that allowed the mass flow rate and skin friction to be recorded simultaneously. The analog signal was limited to the calibration range, but the meter gave a digital reading on a display up to 1200 SCFM. The digital reading was used to estimate ALDR critical fluxes at higher speeds. These points are clearly displayed in the paper as only estimates of the actual value.

The LCC facility was also able to provide tunnel pressure and temperature signals that were recorded simultaneously with the mass flow rate and skin friction. The pressure and temperature signals were measured at the top of the test section and were used to calculate the volumetric flux of air over the HIPLATE.

Results for Air Layer Drag Reduction over Rough Surfaces: Analysis of drag reduction potential are presented in terms of percent drag reduction, %DR as defined by equation (4). To determine %DR for each phase numerous ramps in speed were recorded to obtain τ_{wo}. Figure 13 shows the baseline skin friction results for Phase IV and Va (smooth plate) and Phase Vb (rough plate). Plotted with the baseline skin friction results is the skin-friction line of Schultz-Grunow (1941). For a more detailed analysis of the smooth plate baseline data for this model see Sanders *et al.* (2006).
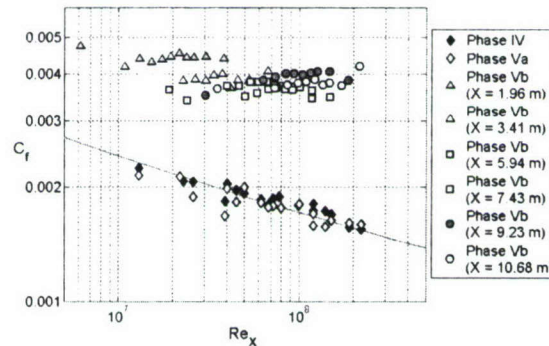
Figure 13: Baseline skin friction data for Phase IV, Va, and Vb. Phase IV and Va were conducted on a smooth test surface and Phase Vb had a roughened test surface.

Downstream persistence of BDR has prevented the application of BDR methods on Naval ships. For this reason during Phase IV methods for improvement of BDR downstream persistence were investigated. Specifically injector dependence, compound injection, bubble size, and boundary layer thickness were studied. As previously stated, two injectors were used during Phase IV, a porous-plate and a slot injector. Figure 14 shows comparisons of the two injectors at three test speeds (6.7, 13.3, and 20 m/s), injection rates ranging from 80 – 640 SCFM, and injection from the first injection location (X_{inj} = 1.38 m). These results show improved drag reduction near the injector with the porous-plate injector, but only marginal improvements on downstream persistence. It should also be noted that the large drag reduction cases (>70% over the entire model) for the 6.7 and 13.3 m/s cases are the results of a transition to ALDR and will be discussed below.

17
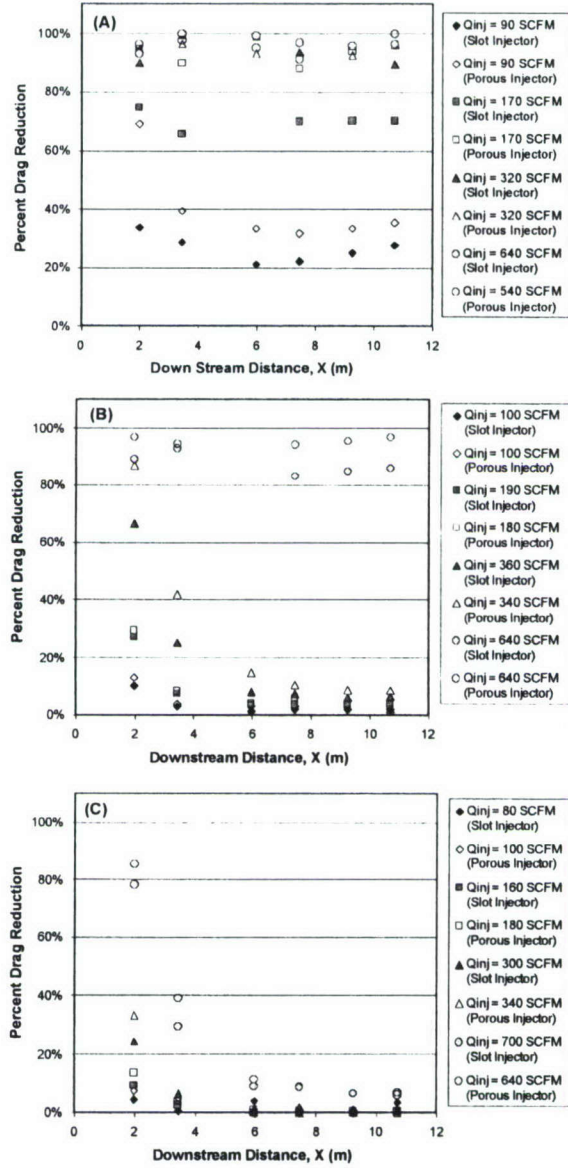
Figure 14: Comparisons of porous and slot injectors located 1.38 m downstream of the leading edge at (A) 6.7 m/s, (B) 13.3 m/s, and (C) 20.0 m/s free-stream speeds.

Compound injection was investigated next to determine if any synergetic effects exist while simultaneously injecting from two injectors. This was accomplished by comparing the percent drag reduction of a single slot injection at X_{inj} = 1.38 m to compound injection with X_{inj1} = 1.38 m and X_{inj2} = 3.73 m with equivalent volumetric flux of air evenly divided between the two injectors. Figure 15 shows the comparisons at three free-stream speeds (6.7, 13.3, and 20 m/s) and 2 nominal total injection rates (180 and 340 SCFM). Results indicate that there was little or no advantage to compound injection.
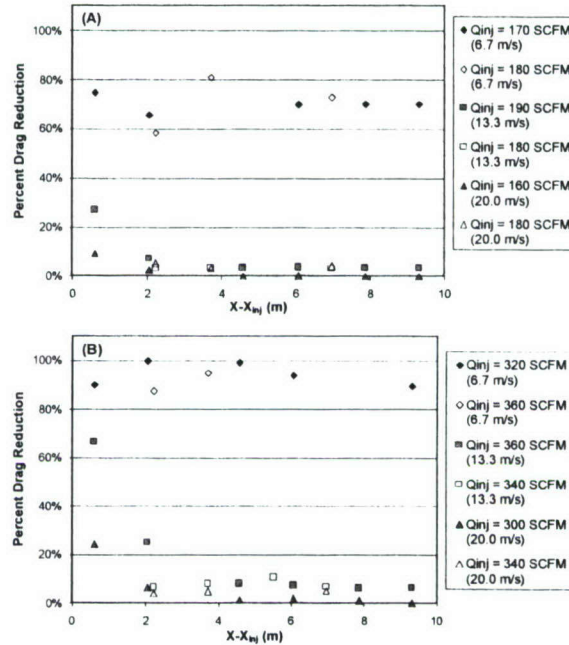
Figure 15: Comparison of compound injection to single injection at nominal injection of (A) 180 SCFM and (B) 340 SCFM. Solid symbols have single injection with X_{inj} = 1.38 m and outlined symbols have compound injection with X_{inj} = 3.73 m.

The influence of bubble size on BDR was investigated by reducing the surface tension. This was accomplished by adding a soluble surfactant (Triton-X-100) to the background tunnel water. The background surfactant concentration was 15 wppm and Winkel *et al.* (2004) showed that this level can reduce the bubble size by a factor of two near the injector. The background surface tension was measured with an in situ tensiometry device, which is described in Lapham *et al.* (1999). The background surface tension without surfactant was measured to be 70 ± 1 dyne/cm and after surfactant was added 50 ± 5 dyne/cm. Figure 16 shows the results using the porous-plate injector located at X_{inj} = 1.38 m, three free-stream speeds (6.7, 13.3, and 20.0 m/s), and injection rate ranging from 90 to 640 SCFM. No significant change in drag reduction was observed with reduced the surface tension.

19
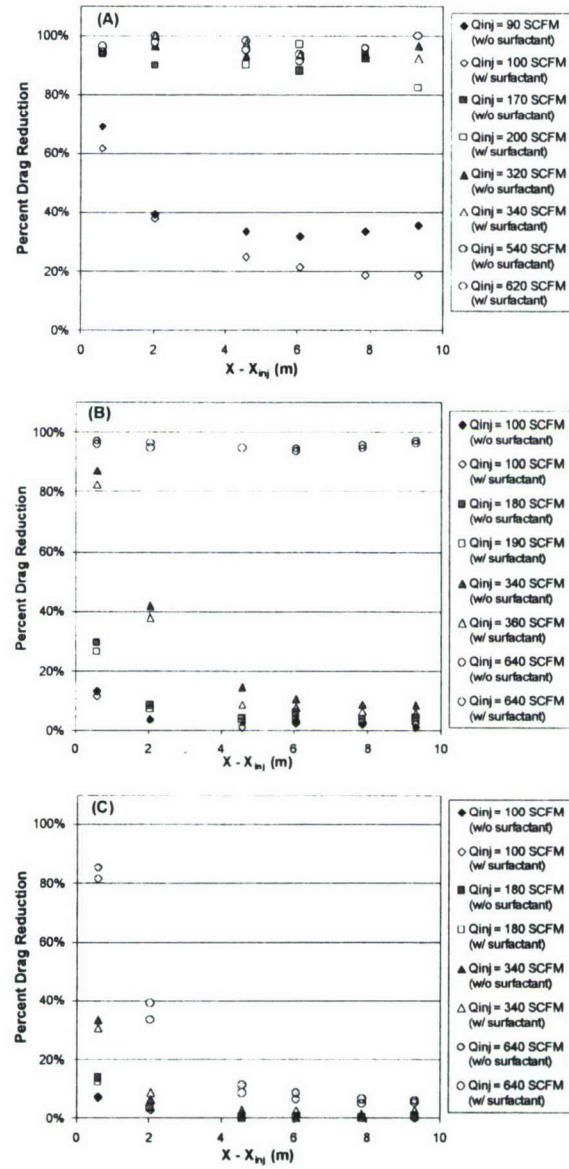
Figure 16: Bubble size comparison at free-stream speed of (A) 6.7 m/s, (B) 13.3 m/s, and (C) 20.0 m/s. Solid symbols are without background surfactant and outlined symbols are with background surfactant.

The influence of the boundary layer thickness on BDR was investigated by injecting from a single downstream location ($X_{inj} = 1.38$ m or $X_{inj} = 3.73$ m) with the Phase IV slot injector. The effect of boundary layer thickness was investigated by plotting percent drag reduction versus X-X_{inj} and comparing the results for upstream only injection with downstream only injection. Figure 17 shows these results and the curves have good collapse for most of the data, which indicates that boundary layer thickness has negligible effect on BDR.
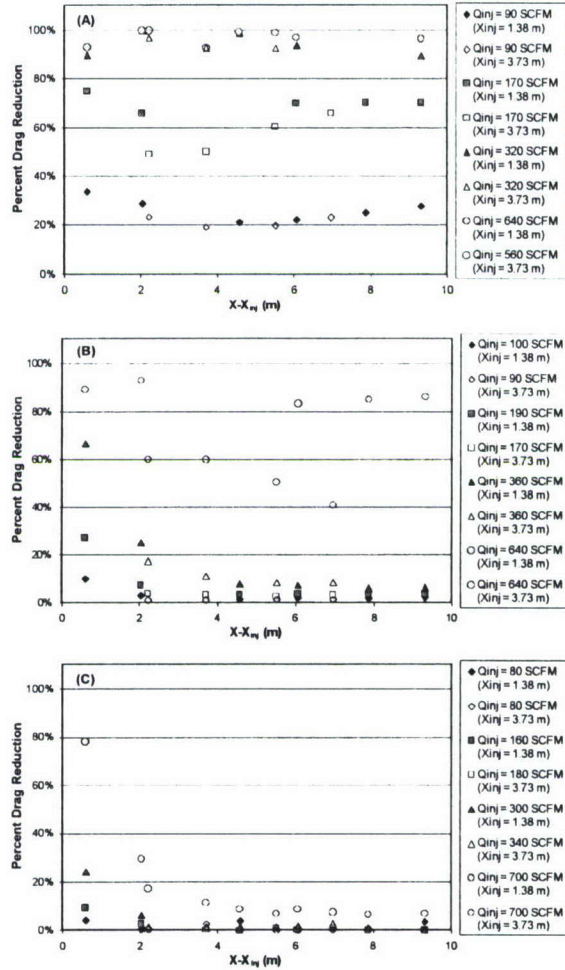
Figure 17: Effect of boundary layer thickness on BDR at (A) 6.7 m/s, (B) 13.3 m/s, and (C) 20.0 m/s. Solid symbols represent injection at X_{inj} = 1.38 m and open symbols at X_{inj} = 3.73 m.

During Phase IV BDR experiments it was observed that under certain flow conditions more than 80% drag reduction was observed on the entire test model. This observation inspired a subset of experiments that consisted of a slow ramp in mass flow rate (5-10 SCFM/s) until greater than 80% drag reduction was observed on all skin friction sensors. It was observed that an abrupt jump occurs in the drag reduction once a critical volumetric flux, Q_{crit}, was reached for a given free-stream speed. This phenomenon was termed ALDR since preliminary data indicate that once Q_{crit} was obtained buoyancy dominated and allowed a layer of air to form on the surface. This sudden transition to ALDR from BDR is shown in Figure 18 with the two furthest downstream skin friction sensors.

Tests were performed to determine the Q_{crit} required to transition to ALDR over a wide range of tunnel speeds. Phase IV investigated four speeds; nominally 6.7, 8.9, 11.1, and 13.3 m/s. Those speeds were repeated in Phase Va plus one additional speed, 15.3 m/s. Attempts were made above 15.3 m/s with no observation of ALDR, presumably due to limitations on the gas delivery system. The 15.3 m/s test condition exceeded the calibration range of the mass flow meter, but an estimate of the required Q_{crit} was determined from the digital display. The Q_{crit} was defined as the volumetric flux required

21

to obtain 95% of the maximum drag reduction observed at the four downstream skin-friction sensors.
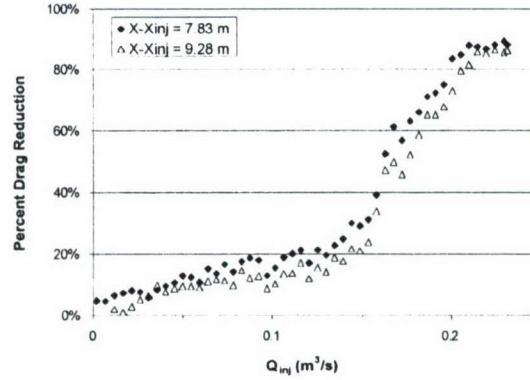
Figure 18: The relatively abrupt transition from BDR to ALDR for nominally 8 m/s tunnel speed with the roughened test surface. The data shown are from the two furthest downstream skin friction drag sensors.

Transition to ALDR was also observed with the roughened model surface at 6.8, 8.0, 9.2, 10.2, 11.3, and 12.5 m/s (11.3 and 12.5 m/s observed ALDR but exceeded the calibration range of the mass flow meter). While ALDR was observed, it required a higher air flux to transition at a given speed than with the smooth plate. Figure 19 shows the critical volumetric flux for Phases IV and V.
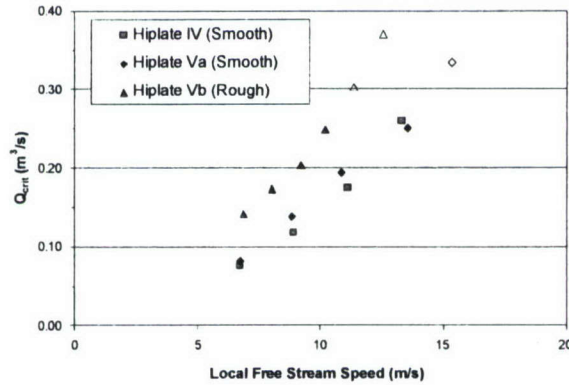
Figure 19: Critical volumetric flux required to transition to ALDR. Outlined symbols correspond to data points that exceeded the mass flow meter calibration range.

During Phase V with the roughened test surface, video was recorded of the injection ramps to observe the transition from BDR to ALDR. The camera was mounted below the test surface and had a view of a fixed location at about 5 meters downstream of the leading edge. Figure 20 shows images from the video at three times during an injection ramp with a tunnel speed of 6.8 m/s. Figure 20a was taken with no air injection and shows the roughened model surface, Figure 20b was taken prior to reaching the critical volumetric flux required to transition to ALDR (i.e. was taken during BDR), and Figure 20c was taken following the transition to ALDR. These images support the view that transition from BDR to ALDR corresponds to a change in flow regimes.

22
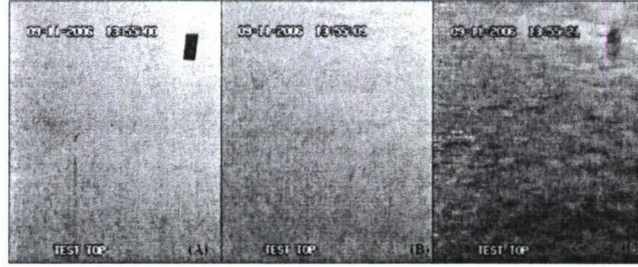
Figure 20: Images from ALDR on the roughened test model at (A) no injection, (B) during BDR, and (C) during ALDR.

Conclusions for Air Layer Drag Reduction over Rough Surfaces: From the drag reduction experiments conducted on the HIPLATE model several conclusions can be made about BDR: 1) Injector geometry has only a marginal impact on downstream persistence; 2) Compound injection (simultaneous gas injection from two injector locations) showed no significant improvement over injection from a single injector; 3) Reducing bubble size by reducing surface tension has little or no effect on downstream persistence of BDR; and 4) Boundary layer thickness did not show significant impact on BDR for the two locations investigated.

These experiments also provided several conclusions about ALDR: 1) Drag reduction by wall-injected gas can be divided into three regions (Region I – BDR zone, Region II – BDR to ALDR transition zone, and Region III – ALDR zone); 2) Transition to ALDR requires a critical volumetric flux of air that is approximately proportional to the square of the free-stream speed; 3) Near-complete drag reduction was observed over the entire model length ($X-X_{inj} \sim 10$ m); and 4) Increasing the surface roughness results in an increase in the critical volumetric flux to transition to ALDR but a stable air layer still forms.

References

Dubief, Y., White, C.M., Terrapon, V.E., Shaqfeh, S.G., Moin, P., and Lele, S.K. (2004) "On the coherent drag-reducing and turbulence enhancing behaviour of polymers in wall flows," *J. Fluid Mech.*, **514**, 271-280.

Etter R. J., Cutbirth, J. M., Ceccio, S. L., Dowling, D. R., & Perlin, M. (2005) "High Reynolds Number Experimentation in the U. S. Navy's William B. Morgan Large Cavitation Channel," Measurement Science and Technology, 16(9), 1701-1709.

Jiménez, J. and Pinelli, A. (1999) "The autonomous cycle of near-wall turbulence," J. Fluid Mech., 389, 335-359.

Lapham, G.S., Dowling, D.R. & Schultz, W.W. (1999) In situ force-balance tensiometry. Experiments in Fluids, Vol. 27, 157-166.

McCormick, M.E. & Battacharyya, R. Drag reduction of a submersible hull by electrolysis. Naval Engineers Journal, Vol. 85, 11-16 (1973)

Merkle, C. & Deutsch, S. Microbubble drag reduction in liquid turbulent boundary layers. Applied Mechanics Review, Vol. 45 (3), 103-127 (1992)

Petrie, H.L., Brungart, T.A., and Fontaine, A.A. (1996) "Drag reduction on a flat plate at high Reynolds number with slot-injected polymer solutions," *Proceedings of the ASME Fluids Engin. Div.*, **237**, 3-9.

Petrie, H.L., Deutsch, S., Brungart, T.A., and Fontaine, A.A. (2003) "Polymer drag reduction with surface roughness in flat-plate turbulent boundary layer flow," *Exps. Fluids*, **35**, 8-23.

Ptasinski, P.K., Boersma, B.J., Nieuwstadt, F.T.M., Hulsen, M.A., Van den Brule, B.H.A.A., and Hunt, J.C.R. (2003) "Turbulent channel flow near maximum drag reduction: simulations, experiments and mechanisms," *J. Fluid Mech.*, **490**, 251-291.

Sanders, W.C., Winkel, E.S., Dowling, D.R., Perlin, M. & Ceccio, S.L. (2006) Bubble friction drag reduction in a high-Reynolds-number flat-plate turbulent boundary layer. Journal of Fluid Mechanics, Vol. 552, 353-380.

Schultz-Grunow, F. (1941) "New frictional resistance law for smooth plates," *NACA* T M, **17**, 1-24.

Sellin R.H.J., Hoyt J.W., Scrivener O. (1982a) "The effect of drag reducing additives on fluid flows and their industrial applications: Part I. Basic aspects," *J. Hydr. Res.*, **20** (1), 29-68.

Sellin R.H.J., Hoyt J.W., Scrivener O. (1982b) "The effect of drag reducing additives on fluid flows and their industrial applications: Part II. Basic aplications and future proposals," *J. Hydr. Res.*, 20 (3), 235-293.

Toms, B.A. (1949) "Some observations on the flow of linear polymer solutions through straight tubes at large Reynolds numbers," *Proceedings of the First International Congress on Rheology.*

Vdovin A.V. and Smol'yakov, A.V. (1978) "Diffusion of polymer solutions in a turbulent boundary layer," *J. App. Mech. And Tech. Phys*, **19**(2), 66-73.

Vdovin A.V. and Smol'yakov, A.V. (1981) "Turbulent diffusion of polymers in a boundary layer," *J. App. Mech. And Tech. Phys*, **22**(4), 98-104.

Virk, P.S. (1975) "Drag Reduction Fundamentals," *AIChE* **21**(4), 625-656.

Warholic, M.D., Massah, H., and Hanratty, T.J. (1999) "Influence of drag-reducing polymers on turbulence: effects of Reynolds number, concentration and mixing," *Exps. Fluids*, **27**, 461-472.

White, C.M., Somandepalli, V.S.R., and Mungal, M.G. (2004) "The turbulence structure of drag reduced boundary layer flow," *Exps. Fluids*, **36**, 62-69.

White, F. M. (1991) *Viscous Fluid Flow*, McGraw Hill, Inc.

Winkel, E.S., Ceccio, S.L., Dowling D.R. & Perlin, M. (2004) Bubble size distributions produced by wall-injection of air into flowing freshwater, saltwater, and surfactant solutions. Experiments in Fluids, Vol. 3, 802-810.

Wu J. and Tulin, M.P. (1972) "Drag reduction by ejecting additive solutions into pure-water boundary layer," *J. Basic Engin., Transactions of the ASME*, **94**, 749-756.

Zalek, S., Beck, R., Ceccio, S.L. & Reed, A. (2004) Drag reduction for high speed ship design. Report to the Office of Naval Research.